Optik - International Journal for Light and Electron Optics 221 (2020) 165403

Contents lists available at ScienceDirect

Optik

journal homepage: www.elsevier.com/locate/ijleo

Original research article

Numerical simulation of GaN/InGaN p-i-n solar cells: Role of interlayers in promoting photovoltaic response

Debashish Pal [a,*], Soumee Das [b]

[a] Department of Material Science and Engineering, Tripura University, India
[b] IBM India Pvt. Ltd., Kolkata, India

ARTICLE INFO

Keywords:
Polarisation
Heterojunction
Trap assisted recombination
Interlayer film (ILF)
InGaN
Solis-1D

ABSTRACT

Numerical simulation has been performed to investigate the GaN/$In_xGa_{1-x}N$ heterojunction p-i-n solar cell. The role of indium composition in the absorber and the presence of polarisation charges have been studied thoroughly. ILF has been proposed at the heterointerface of p-GaN/i-$In_xGa_{1-x}N$ which proved to be beneficial in overcoming the undesirable effects of charge transport across heterojunction by reducing SRH recombination, especially prevalent at high indium compositions. The simulations were conducted at low and high indium compositions and the photovoltaic properties were examined using Solis-1D Semiconductor Device Simulator.

1. Introduction

Reducing the fabrication cost, time and complexity of solar cells have become a necessity these days because of the elaborate choices available in the form of materials and structures. These difficulties associated with fabrication can be overcome by first gaining some insights into the operation and behaviour of the devices by the use of suitable simulation programs. In general, solar cell simulation programs assist in evaluating the electronic and optical responses based on alterations in various parameters which are of significant importance.

The III-nitride semiconductor materials including their alloys are direct bandgap materials which covers the entire visible range of the solar spectrum. Specifically, the InGaN alloy finds application in solar cells since its bandgap can be tuned (0.64 eV–3.4 eV) by varying the indium composition [1,2]. Furthermore, InGaN has a high absorption coefficient ~10^5/cm [3], high radiation resistance, increased carrier mobility, good thermal conductivity and low effective mass which makes it a prospective material for solar photovoltaics [4].

Notwithstanding the several advantages, progress in achieving desirable efficiency for InGaN solar cells have encountered setbacks due to trouble achieving highly crystalline In-rich absorber layers [5]. Because III-nitride materials have wurtzite structures they are usually grown over sapphire substrates to lessen the detrimental effects of lattice mismatch. Studies have revealed that there is an inverse relationship between the thickness of the InGaN absorber and the indium concentration [6]. Also, with increase in indium composition, the degree of lattice mismatch of absorber with GaN template promotes the possibility of non radiative recombination due to high defect density formation [7]. The formation of a heterojunction resulting from the large difference in bandgap energy at the interface of GaN and InGaN also disrupts the flow of charge carriers. High internal polarisation particularly spontaneous and strain generated piezoelectric polarisations results in interfacial charges in III-nitride heterostructures grown on the c-plane [8,9]. The

* Corresponding author.
E-mail address: pal.debashish@gmail.com (D. Pal).

https://doi.org/10.1016/j.ijleo.2020.165403
Received 11 May 2020; Accepted 7 August 2020
Available online 10 August 2020

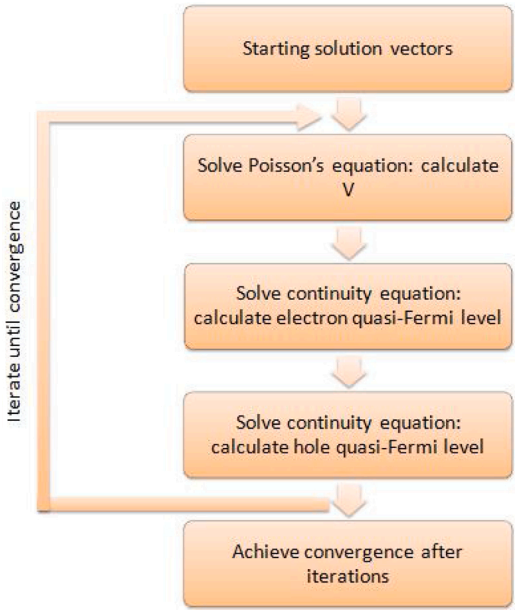

Fig. 1. Diagrammatic flow that solves the discretized non-linear PDEs using Newton-Raphson algorithm.

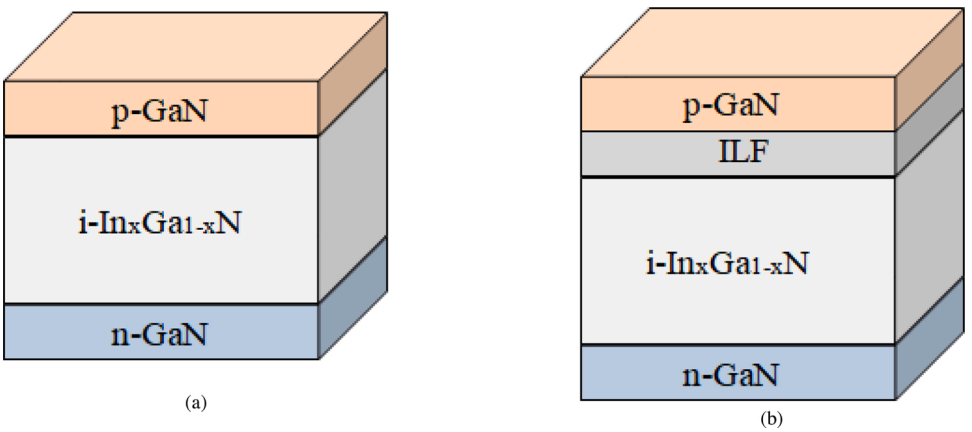

Fig. 2. Schematic diagram of the cell (a) without ILF (b) with ILF.

interfacial charge induced field hinders carrier extraction by opposing the built-in electric field. Additionally, it is difficult to obtain p^+-type doping in InGaN alloys because of inadequate solubility of acceptor atoms and because of large n-type background doping due to the presence of defects [10].

The issue of carrier collection was addressed in a numerical investigation by the incorporation of highly doped step-grading interlayers at the GaN-InGaN hetero-interface. The p-GaN doping level was kept low in order to diminish the polarisation and potential barrier [11]. Furthermore, it was suggested that for smaller degrees of relaxation, the inclusion of polarisation compensating interlayers enhances the electric field strength inside the absorber which is favourable for carrier extraction [12]. It was also established that the presence of polarisation matched layers (PML) at the GaN-InGaN interface results in better hole extraction from the absorber layer. Also for low p-type doping in GaN along with higher indium amount in absorber, greater PML thickness is inevitable [13].

In this paper, a thorough numerical computational analysis has been performed by Solis-1D Semiconductor Device Simulator [14] which can take into account spontaneous and piezoelectric polarisation in III-nitride wurtzite structures. The performance has been evaluated for a GaN-InGaN heterojunction solar cell having p-i-n configuration with 10%, 15%, 20% and 25% indium content in the absorber. The cell structure was first optimised ignoring the effect of polarisation. Subsequently the polarisation factor was taken into consideration and its outcome on various parameters was discussed. Appropriate bandgap tuned interlayer film (ILF) was introduced to alleviate the shortcomings associated with polarisation and heterojunction formation.

Table 1
Basic material parameters used in the simulation of the cell. E_G, χ, N_C, N_V, ε_r and β represents the bandgap energy, electron affinity, conduction band density of states, valence band density of states, relative permittivity and the direct recombination parameter respectively.

	E_G (eV)	χ (eV)	N_C (/cm^3)	N_V (/cm^3)	ε_r	β (cm^3/s)
GaN	3.4	4.1	1.2×10^{18}	4.1×10^{19}	8.9	1.1×10^{-8}
InN	0.7	5.26	9×10^{17}	5.3×10^{19}	15.3	2.0×10^{-10}

Table 2
Experimental value of the polarisation coefficients [20].

	e_{31} (C/m^2)	e_{33} (C/m^2)	c_{13} (GPa)	c_{33} (GPa)
GaN	−0.34	0.67	100	392
InN	−0.41	0.81	94	200

2. Numerical parameters and cell structure

Using the drift-diffusion model the Poisson's and continuity equations are solved to determine the potential, electron and hole quasi-Fermi levels. The partial differential equations (PDEs) are discretized with the Scharfetter-Gummel method and the equations are solved thereafter using the Gummel iterative decoupled method or the Newton method using the Newton-Raphson algorithm. For tightly coupled drift-diffusion equations the Gummel method converges slowly, in which case the Newton method proves effective. Fig. 1 is a general sequential representation of the three equations solved by Solis program until convergence is reached.

The p-i-n configuration used in the study is shown in Fig. 2 which represents the schematic diagram of (a) basic and the (b) modified solar cell structures.

The primary parameters used in the simulation are listed in Table 1. [14–16]

Because of compositional change and menial crystal quality compared to InN and GaN, the lifetime of the charge carriers in $In_xGa_{1-x}N$ absorber layer is assumed to be lesser (~1 ns). The electron and hole mobilities are calculated using the relation [17]:

$$\mu_i(N) = \mu_{\min,i} + \frac{\mu_{\max,i} - \mu_{\min,i}}{1 + \left(\frac{N}{N_{g,i}}\right)^{\gamma_i}} \tag{1}$$

where, i represents both electrons and holes. Here, μmax, μmin, N_g and γ_i are semiconductor material specific constants and N is the doping concentration. These values are tabulated in Brown et al. 2010.

The absorption coefficient as a function of energy for $In_xGa_{1-x}N$ alloy is given by:

$$\alpha(E) = 10^5 \sqrt{a(E - E_G) + b(E - E_G)^2}\,\mathrm{cm}^{-1} \tag{2}$$

where, the values a and b are dimensionless fitting parameters [18].

The temperature dependent bandgap energies of the ternary semiconductors are calculated using the formula (Vurgaftman et al. 2001):

$$E_G(In_xGa_{1-x}N) = x.E_G(InN) + (1 - x).E_G(GaN) - b.x.(1 - x) \tag{3}$$

where, $E_G(InN)$ and $E_G(GaN)$ values are given in Table 1. The bowing parameter b of E_G is 1.43 eV while it is set at 0.5 eV for χ.

The total polarisation in III-nitride semiconductors is the sum of two contributions: spontaneous and piezoelectric [8]:

P_{total}=*Polarisation scale* x (P_{sp}+P_{pi})

$$P_{pi} = \sum_j e_{ij}\varepsilon_j = e_{33}\varepsilon_3 + e_{31}(\varepsilon_1 + \varepsilon_2)$$

$$\varepsilon_3 = -2\frac{c_{13}}{c_{33}}\left(\frac{a - a_0}{a_0}\right) \text{ and } \varepsilon_1 = \varepsilon_2 = \left(\frac{a - a_0}{a_0}\right) \tag{4}$$

where, a is the lattice parameter of the strained layer and a_0 that of the strained layer. e_{31}, e_{32} are piezoelectric coefficients (C/m^2) and c_{13}, c_{33} are the elastic coefficients (GPa). The values of the coefficients used in the simulation are derived from experimental data and are presented in Table 2. The polarisation scale value varies between -10 to +10 with 0 indicating no polarisation. This parameter is useful in investigating the effect of spontaneous and piezoelectric polarisation on the device.

The top and bottom contacts were assumed to be perfectly ohmic with a relatively high surface recombination velocity of 1×10^9cm/s for both electrons and holes. Simulations were performed under AM1.5 G one sun illumination condition having an intensity of 100 mW/cm^2 at an operating temperature of 300 K.

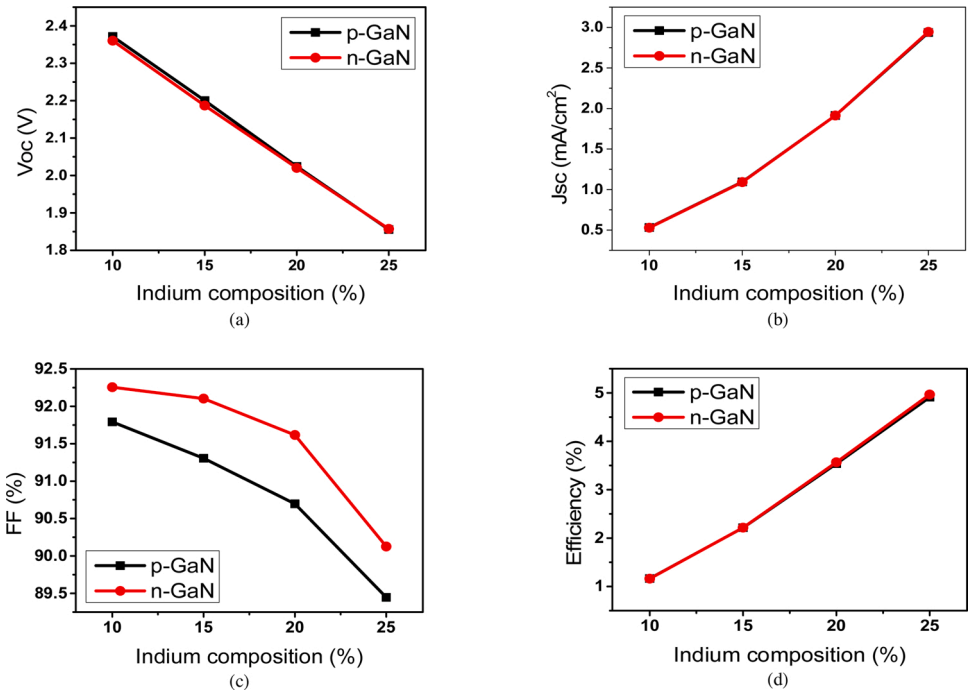

Fig. 3. (a) V_{OC} (b) J_{SC} (c) FF (d) η curves for optimised p-GaN and n-GaN thickness and doping density upon AM 1.5 G one sun illumination (P = 0).

Table 3
Summary of the output parameters after optimisation of the p-GaN and n-GaN layers.

p-GaN	Doping density (/cm^3)	5×10^{17}	5×10^{18}	5×10^{18}	5×10^{18}
	Thickness (nm)	150	150	150	150
i-InGaN absorber	Composition (%)	10	15	20	25
	Thickness (nm)	200	200	200	200
n-GaN	Doping density (/cm^3)	5×10^{18}	1×10^{18}	1×10^{18}	1×10^{18}
	Thickness (nm)	1000	1000	1000	1000
Output characteristics	V_{OC} (V)	2.37	2.19	2.02	1.86
	J_{SC} (mA/cm^2)	1.91	1.09	1.91	2.95
	FF (%)	91.79	92.10	91.62	90.13
	η (%)	1.16	2.22	3.57	4.97

3. Results and discussion

For optimisation of the cell (Fig. 2 (a)) the p-GaN thickness and doping concentration is varied together with the thickness of i-InGaN absorber layer. The width of the p-GaN layer was varied from 50 nm to 150 nm and the doping level was varied from 5×10^{17}/cm^3 to 5×10^{18}/cm^3. While the doping concentration was being altered the width was kept constant and vice-versa. Similarly, while the above parameters were unaltered the thickness of the absorber layer was varied from 50 to 200 nm. These studies were conducted for indium compositions of 10%, 15%, 20% and 25%. It is to be noted that during the course of these studies the width and doping level of n-GaN template was held constant at 1 μm and 5×10^{18}/cm^3. As expected, the cell attained highest efficiency when the width of the absorber was 200 nm, as thicker absorbers allow more photons, increasing the photocurrent density. It was also observed that for lower indium content (~10%) the efficiency was highest for a lower doping level (~5×10^{17}/cm^3). On the other hand, for greater indium compositions (~15%, 20% and 25%) the efficiencies peaked for high doping levels (~5×10^{18}/cm^3). Additionally, in general the efficiencies attained a maximum for thicker (~150 nm) p-GaN layer.

The same studies were repeated for n-GaN template layer for p-GaN doping density of 5×10^{18}/cm^3 and width 150 nm. The n-GaN width was held constant at 1 μm while its doping concentration was varied from 1×10^{18}/cm^3 to 5×10^{18}/cm^3 along with the absorber indium concentration. Interestingly it was noted that for small indium concentration (~10%) the efficiency decreased with increase in doping concentration. For high indium contents (~15%, 20% and 25%) the opposite outcome is observed. In general, the trend in variation of parameters was very similar in nature to that already discussed in case of p-GaN optimisation. A summary of the results are presented in Fig. 3, which demonstrate the variation of V_{OC}, J_{SC}, FF and η as a function of absorber layer indium amount.

The optimised cell structure for the baseline solar cell without the ILF layer (Fig. 2 (a)) is presented in Table 3.

Also, as discussed, because of the complications associated with high doping levels of p-GaN layer, investigations were carried out

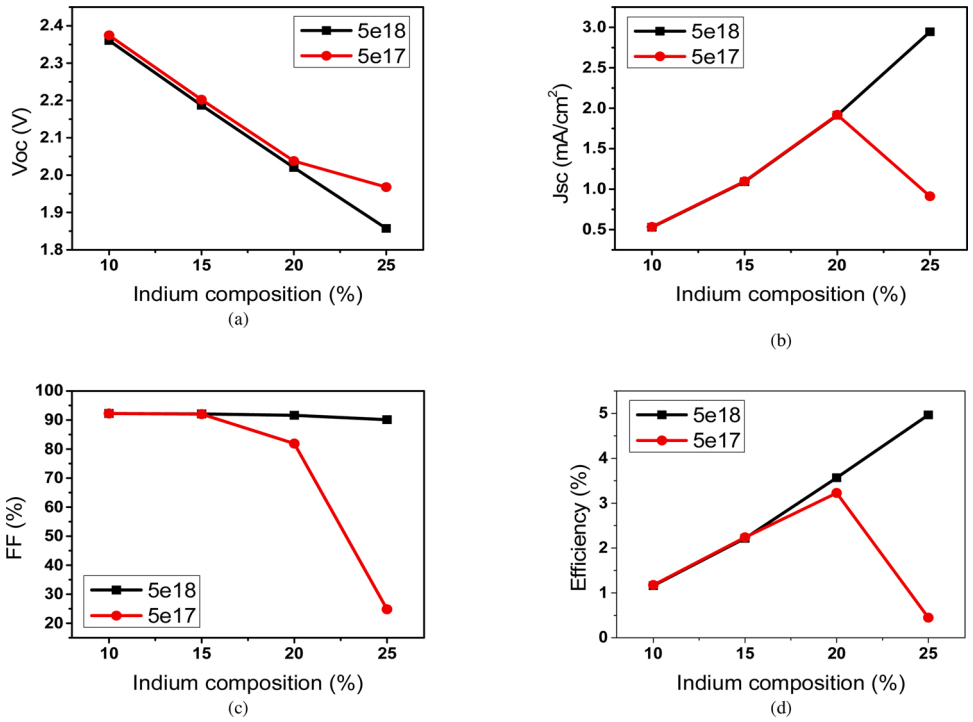

Fig. 4. (a) V_{OC} (b) J_{SC} (c) FF (d) η curves for low and high p-GaN doping concentration upon AM 1.5 G one sun illumination (P = 0).

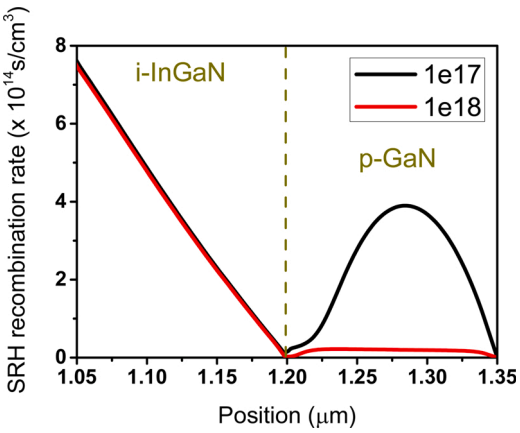

Fig. 5. SRH recombination rate inside the p-GaN layer for low and high impurity concentration in case of absorber indium content = 10% upon AM 1.5 G one sun illumination (P = 0).

to demonstrate the impact of experimentally feasible doping levels as compared to that of theoretically favourable doping concentrations. As shown in Fig. 4 for high doping level (5×10^{18}/cm^3), V_{OC} decreases significantly while J_{SC} and η increases with increase in indium proportion. For relatively low doping (5×10^{17}/cm^3) however, this trend is observable for indium amounts below 20%. In case of pronounced indium amount (greater than 20%), J_{SC} and η decreases due to enhanced trap assisted recombination, which is also reflected in the FF curve. This claim can be substantiated by recording the recombination rate inside the p-GaN layer at experimentally feasible doping level (5×10^{17}/cm^3) under AM 1.5 G illumination as demonstrated in Fig. 5.

The effect of polarisation will be accounted for in subsequent investigations and its detrimental ramifications on charge collection and efficiency will be presented in detail. It is to be noted that during the course of further analysis the p-GaN impurity concentration and width were held constant at 5×10^{18}/cm^3 and 150 nm respectively. At the same time, the n-GaN doping concentration and thickness were fixed at 1×10^{18}/cm^3 and 1 μm respectively. As discussed earlier, the total electric field intensity inside the absorber layer subsides due to the presence of polarisation charge induced field which opposes the natural built-in field. The drift velocity of the charge carriers inside the depletion region therefore reduces due to decrease in effective field strength. The comparison of electrostatic

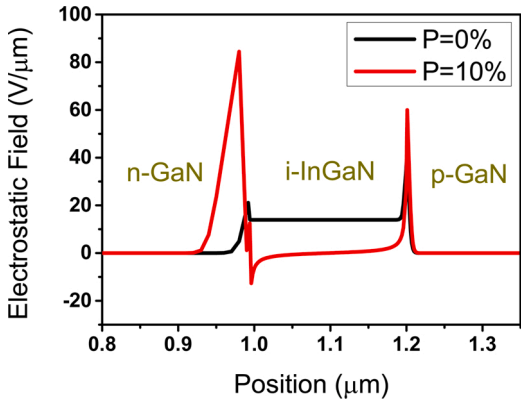

Fig. 6. Electrostatic field distribution of the original cell for degree of polarisation = 0% and 10% with 10% indium content.

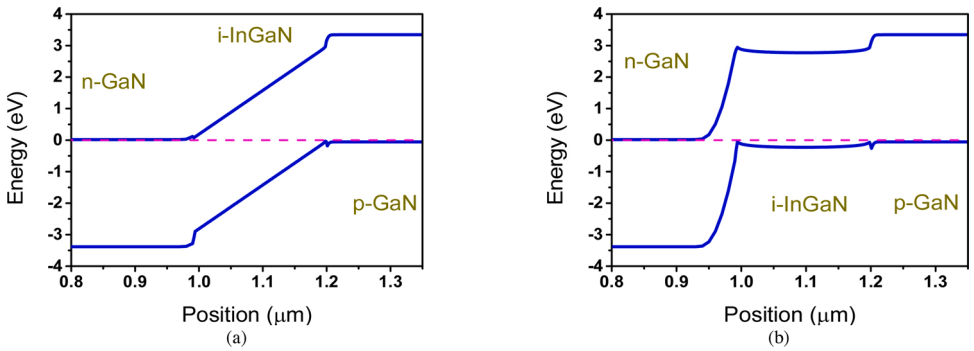

Fig. 7. (a) and (b) Energy band diagram of the cell at equilibrium for absorber indium content = 10% and degree of polarisation = 0% and 10% respectively.

field distribution inside the cell is shown in Fig. 6 which validates the decrease in electric field intensity inside the absorber under P = 10%. This phenomenon can also be explained in terms of the energy band diagram as shown in the Fig. 7. It can be observed that the cell having P = 10% has an almost horizontal energy band at the absorber, which is indicative of the compensation of electric field by polarisation charges. Therefore the photogenerated charge carriers are unable to drift over the potential barrier at the hetero-junction before recombination takes place. Interestingly however, as evident from Fig. 6, at P = 10% the electric field at n-GaN/i-InGaN interface expiates for the loss in electric field strength inside the absorber. This observation demanded exploring the dependence of electric field at the interfaces of various layers for different degrees of polarisation.

Upon closer analysis it was found that the extent of polarisation had no impact on the electric field distribution at the n-GaN/i-InGaN junction at constant indium composition. However, this was in contrast to the effect of polarisation at the p-GaN/i-InGaN interface, which demonstrated greater electric fields for higher polarisation degrees (Fig. 8 (a) and (b)). These results may be attributed to distortion of electric field at the interface due to the polarisation charges. It therefore became imperative to also study the effect of indium concentration at the interfacial field distribution for fixed polarisation. The effect of strained layer on the electrostatic field is again found to be dominant at the p-GaN/i-InGaN interface compared to the n-GaN/i-InGaN junction (Fig. 8 (c) and (d)). These results may also be ascribed to the higher impurity doping concentration for p-GaN layer ($5 \times 10^{18}/cm^3$) in contrast to n-GaN layer ($1 \times 10^{18}/cm^3$).

Furthermore, simulations were performed to probe the performance of the cell at two different degrees of polarisation (P = 10% and 20%), varying the indium compositions. The results are presented in Fig. 9. For retaining better efficiencies cells with higher indium compositions (≥20%) are preferable. It is apparent that in general the performance of the original structure worsens when the degree of polarisation increases. The efficiencies for both degrees of polarisation attain a maximum value for a moderate indium composition of 20%. When the degree of polarisation is decreased from 20% to 10% the efficiency of the cell for 20% indium content improves by 1255%. Therefore, in order to compensate for these undesired functioning of the original cell, especially for high indium content, interlayer film (ILF) are presented between the p-GaN and absorber layers as shown in Fig. 2(b). The ILF helps in negating the detrimental effects of polarisation in solar cells. It was assumed that the ILF has an acceptor doping concentration equal to that of the p-GaN layer ($5 \times 10^{18}/cm^3$) and an indium composition half as that of the absorber. In addition, for the sake of simplicity investigations were carried out at a fixed polarisation of 10% with absorber indium compositions of 20% and 25%. Simulation of the modified structure was performed to determine the optimum ILF width. A verification of the improved performance can be easily deduced by comparing Fig. 7(b) with Fig. 10. It is clear that the energy band of the cell at the absorber has slanted by a considerable amount due to

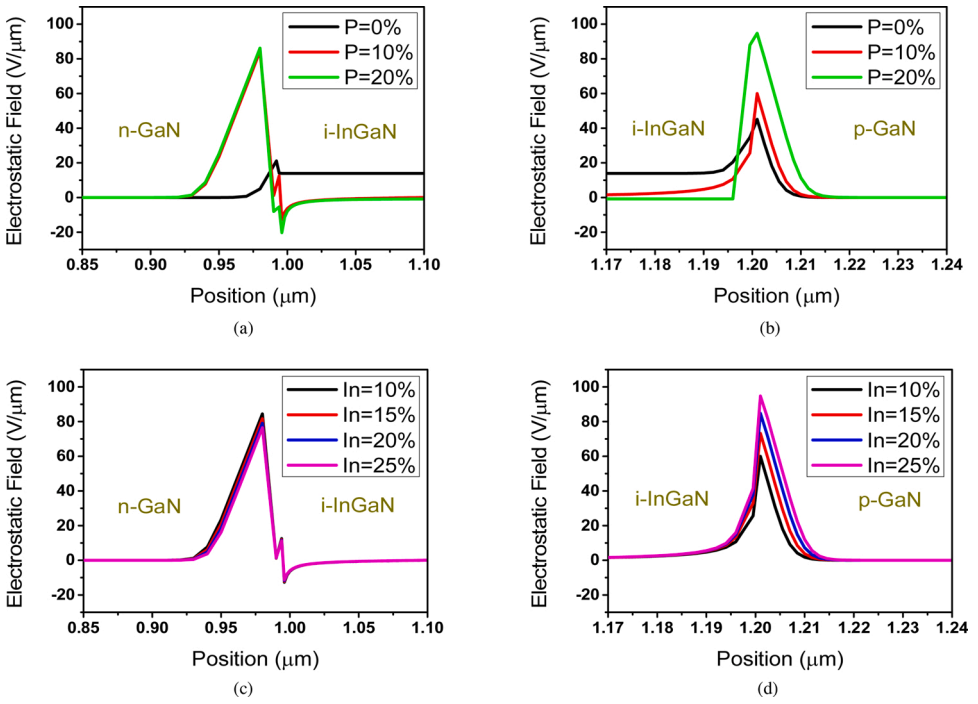

Fig. 8. Electrostatic field distribution at (a), (c) n-GaN/i-InGaN interface for polarisation degree = 0%, 10%, 20% and indium composition = 10%, 15%, 20%, 25% respectively (b), (d) p-GaN/i-InGaN interface for polarisation degree = 0%, 10%, 20% and indium composition = 10%, 15%, 20%, 25% respectively.

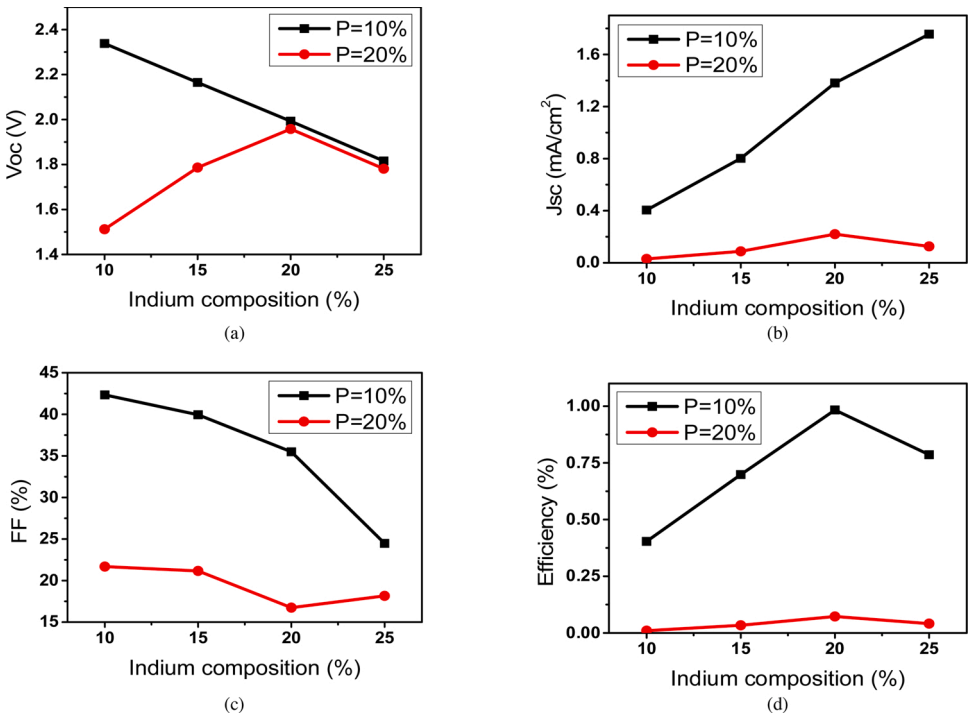

Fig. 9. (a) V_{OC} (b) J_{SC} (c) FF (d) η curves for the original cell structure with P = 10% and 20% under one sun AM 1.5 G illumination.

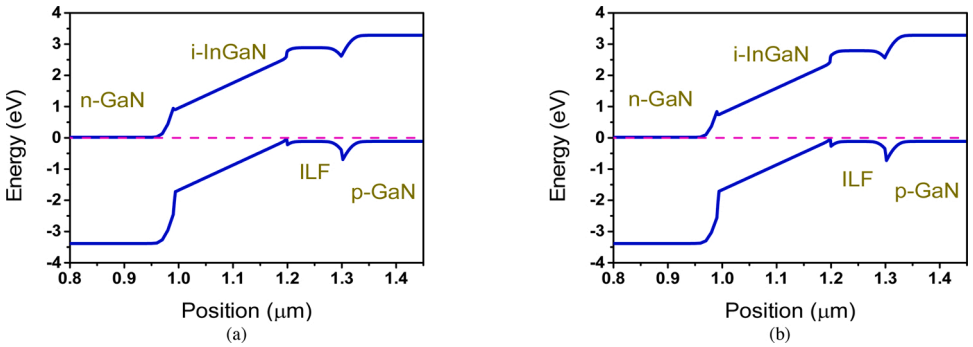

Fig. 10. (a) and (b) Energy band diagram of the cell at equilibrium for absorber indium content = 20% and 25% with degree of polarisation = 10%.

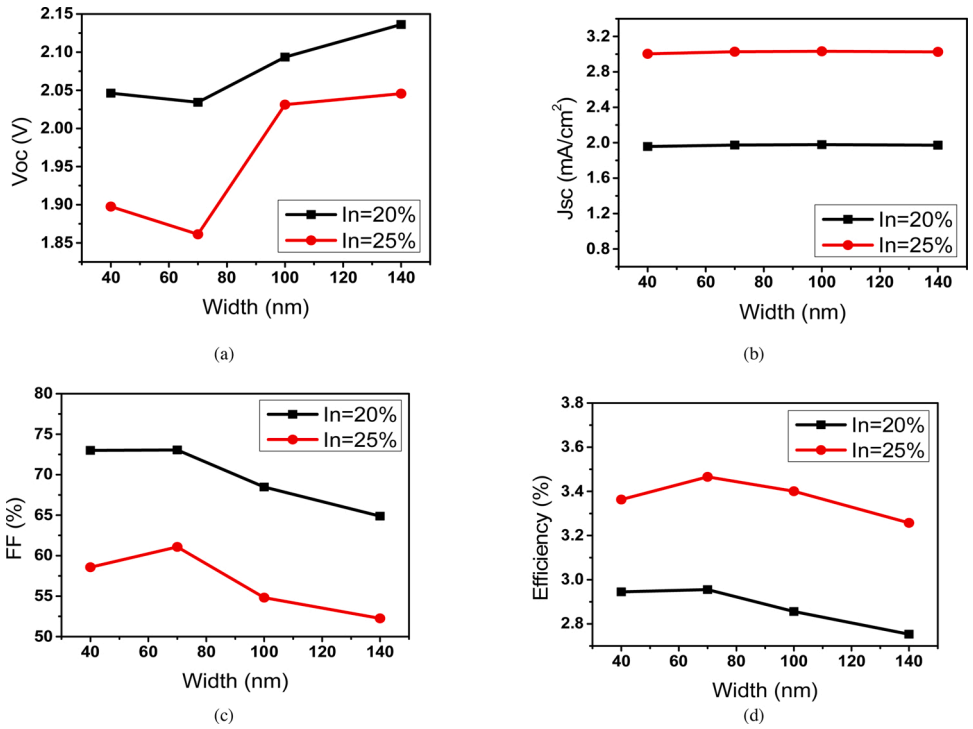

Fig. 11. (a) V_{OC} (b) J_{SC} (c) FF (d) η curves for the modified cell structure after the incorporation of ILF with 20% and 25% indium content under one sun AM 1.5 G illumination (P = 10%).

the presence of ILF which aids the drift of photogenerated carriers before recombination takes place. This band inclination lowers the potential requirement for charge extraction and increases J_{SC} which in turn is also reflected as improvement in η. Based on the curves obtained (Fig. 11) it can be inferred that, in general greater indium compositions have an unfavourable impact on V_{OC} and FF, in case of the structure incorporating ILF layer. On the other hand an opposite effect of composition is observed in case of J_{SC} and η. It is also obvious from the curves that for higher indium compositions the use of thicker ILF layers adversely affects the efficiency of the modified cell. It must be emphasised herein that the values of theoretical efficiency obtained in this work are lower as compared to similar work reported in the recent past [13,21]. This is because the surface recombination rate considered in the present work has been assumed to be very high ($\sim 1 \times 10^9$cm/s).

4. Conclusion

To sum up, in order to extract better efficiency yield from the original structure with no polarisation: (a) thicker (~150 nm) p-type material is preferable (b) for p-type material absorber indium compositions greater than 20%, higher doping concentration ($\sim 5 \times 10^{18}$/cm^3) is necessary to overcome the loss due to trap assisted recombination (c) for n-type epitaxial layer, impurity concentration should be 1×10^{18}/cm^3 for high indium content absorber material. Because polarisation is inevitable, therefore better

conversion efficiency can be expected from the original structure by the inclusion of ILF. The proposed structure shows improved conversion efficiency if the following conditions are met: (a) the acceptor impurity level of the ILF is expected to be equal to that of the p-type layer ($\sim 5 \times 10^{18}/cm^3$) (b) the indium proportion in the ILF layer should be half as that of p-type material (c) for high indium content in the absorber ($\geq$20%), use of thicker ILF layers is to be avoided. Moreover any indium proportion and any degree of polarisation (greater than 0%) have no effect on the electrostatic field at n-GaN/i-InGaN interface. However this is not the case at the p-GaN/i-InGaN interface as higher degree of polarisation and greater indium composition intensifies the electric field.

Declaration of Competing Interest

The authors declare that they have no known competing financial interests or personal relationships that could have appeared to influence the work reported in this paper.

References

[1] W. Walukiewicz, J.W. Ager, K.M. Yu, Z. Liliental-Weber, J. Wu, S.X. Li, R.E. Jones, J.D. Denlinger, Structure and electronic properties of InN and In-rich group III-nitride alloys, J. Phys. D Appl. Phys. 39 (2006), https://doi.org/10.1088/0022-3727/39/5/R01.
[2] J. Wu, When group-III nitrides go infrared: New properties and perspectives, J. Appl. Phys. 106 (2009), https://doi.org/10.1063/1.3155798.
[3] R.M. Farrell, C.J. Neufeld, S.C. Cruz, J.R. Lang, M. Iza, S. Keller, S. Nakamura, S.P. Denbaars, U.K. Mishra, J.S. Speck, High quantum efficiency InGaN/GaN multiple quantum well solar cells with spectral response extending out to 520 nm, Appl. Phys. Lett. 98 (2011), https://doi.org/10.1063/1.3591976, 2011–2014.
[4] J. Wu, W. Walukiewicz, K.M. Yu, W. Shan, J.W. Ager, E.E. Haller, H. Lu, W.J. Schaff, W.K. Metzger, S. Kurtz, Superior radiation resistance of In 1-xGa xN alloys: Full-solar-spectrum photovoltaic material system, J. Appl. Phys. 94 (2003) 6477–6482, https://doi.org/10.1063/1.1618353.
[5] I.H. Ho, G.B. Stringfellow, Solid phase immiscibility in GaInN, Appl. Phys. Lett. 69 (1996) 2701–2703, https://doi.org/10.1063/1.117683.
[6] D. Holec, P.M.F.J. Costa, M.J. Kappers, C.J. Humphreys, Critical thickness calculations for InGaN/GaN, J. Cryst. Growth 303 (2007) 314–317, https://doi.org/10.1016/j.jcrysgro.2006.12.054.
[7] D. Cherns, S.J. Henley, F.A. Ponce, Edge and screw dislocations as nonradiative centers in InGaN/GaN quantum well luminescence, Appl. Phys. Lett. 78 (2001) 2691–2693, https://doi.org/10.1063/1.1369610.
[8] F. Bernardini, V. Fiorentini, D. Vanderbilt, Spontaneous polarization and piezoelectric constants of III-V nitrides, Phys. Rev. B - Condens. Matter Mater. Phys. 56 (1997) R10024–R10027, https://doi.org/10.1103/PhysRevB.56.R10024.
[9] V. Fiorentini, F. Bernardini, O. Ambacher, Evidence for nonlinear macroscopic polarization in III-V nitride alloy heterostructures, Appl. Phys. Lett. 80 (2002) 1204–1206, https://doi.org/10.1063/1.1448668.
[10] S. Fischer, C. Wetzel, E.E. Haller, B.K. Meyer, doping in GaN—acceptor binding energies, Appl. Phys. Lett. 67 (1995) 1298–1300.
[11] Y.K. Kuo, J.Y. Chang, Y.H. Shih, Numerical study of the effects of hetero-interfaces, polarization charges, and step-graded interlayers on the photovoltaic properties of (0001) face GaN/InGaN p-i-n solar cell, IEEE J. Quantum Electron. 48 (2012) 367–374, https://doi.org/10.1109/JQE.2011.2181972.
[12] J.-Y. Chang, B.-T. Liou, H.-W. Lin, Y.-H. Shih, S.-H. Chang, Y.-K. Kuo, Numerical investigation on the enhanced carrier collection efficiency of Ga-face GaN/InGaN p-i-n solar cells with polarization compensation interlayers, Opt. Lett. 36 (2011) 3500, https://doi.org/10.1364/ol.36.003500.
[13] B. Saini, S. Adhikari, S. Pal, A. Kapoor, Polarization compensation at low p-GaN doping density in InGaN/GaN p-i-n solar cells: Effect of InGaN interlayers, Superlattices Microstruct. 107 (2017) 127–135, https://doi.org/10.1016/j.spmi.2017.04.014.
[14] S. Ould Saad Hamady, Solis: a modular, portable, and high-performance 1D semiconductor device simulator, J. Comput. Electron. (2020), https://doi.org/10.1007/s10825-020-01477-7.
[15] J.W. Slotlnxm, Measurements of bandgap narrowing, J Solid State Electron. 19 (1976) 857–862.
[16] Q. Chen, J.W. Yang, A. Osinsky, S. Gangopadhyay, B. Lim, M.Z. Anwar, M. Asif Khan, D. Kuksenkov, H. Temkin, Schottky barrier detectors on GaN for visible-blind ultraviolet detection, Appl. Phys. Lett. 70 (1997) 2277–2279, https://doi.org/10.1063/1.118837.
[17] T.T. Mnatsakanov, M.E. Levinshtein, L.I. Pomortseva, S.N. Yurkov, G.S. Simin, M.A. Khan, Carrier mobility model for GaN, Solid. Electron. 47 (2003) 111–115, https://doi.org/10.1016/S0038-1101(02)00256-3.
[18] G.F. Brown, J.W. Ager, W. Walukiewicz, J. Wu, Finite element simulations of compositionally graded InGaN solar cells, Sol. Energy Mater. Sol. Cells 94 (2010) 478–483, https://doi.org/10.1016/j.solmat.2009.11.010.
[20] J. Piprek, Semiconductor Optoelectronic Devices: Introduction to Physics and Simulation, 2003, https://doi.org/10.1016/C2009-0-22633-X.
[21] Y.-K. Kuo, J.-Y. Chang, S.-H. Yen, Numerical investigation on the structural characteristics of GaN/InGaN solar cells, Physics, Simulation, Photonic Eng. Photovolt. Devices II. 8620 (2013) 862021, https://doi.org/10.1117/12.2003716.